◆ Human Brain Mapping 39:54–71 (2018) ◆

Reduced Striato-Cortical and Inhibitory Transcallosal Connectivity in the Motor Circuit of Huntington's Disease Patients

Clara Garcia-Gorro,[1,2] Ruth de Diego-Balaguer,[1,2,3,4] Saul Martínez-Horta,[5,6] Jesus Pérez-Pérez,[5,6] Jaime Kulisevsky,[5,6,7] Nadia Rodríguez-Dechicha,[8] Irene Vaquer,[8] Susana Subira,[8,9] Matilde Calopa,[10] Esteban Muñoz,[11,12,13] Pilar Santacruz,[11] Jesús Ruiz-Idiago,[14] Celia Mareca,[14] Nuria Caballol,[15] and Estela Camara [1,2]*

[1]Cognition and Brain Plasticity Unit, IDIBELL (Institut d'Investigació Biomèdica de Bellvitge), L'Hospitalet de Llobregat, Barcelona, Spain
[2]Department of Cognition, Development and Educational Psychology, University of Barcelona, Barcelona, Spain
[3]The Institute of Neurosciences of the University of Barcelona, Barcelona, Spain
[4]ICREA (Catalan Institute for Research and Advanced Studies), Barcelona, Spain
[5]Movement Disorders Unit, Department of Neurology, Biomedical Research Institute Sant Pau (IIB-Sant Pau), Hospital de la Santa Creu i Sant Pau, Barcelona, Spain
[6]CIBERNED (Center for Networked Biomedical Research on Neurodegenerative Diseases), Carlos III Institute, Madrid, Spain
[7]Universidad Autónoma de Barcelona, Barcelona, Spain
[8]Hestia Duran i Reynals, Hospital Duran i Reynals, Hospitalet de Llobregat, Barcelona, Spain
[9]Department of Clinical and Health Psychology, Universitat Autònoma de Barcelona, Barcelona, Spain
[10]Movement Disorders Unit, Neurology Service, Hospital Universitari de Bellvitge, L'Hospitalet de Llobregat, Barcelona, Spain
[11]Movement Disorders Unit, Neurology Service, Hospital Clínic, Barcelona, Spain
[12]IDIBAPS (Institut d'Investigacions Biomèdiques August Pi i Sunyer), Barcelona, Spain
[13]Facultat de medicina, University of Barcelona, Barcelona, Spain
[14]Hospital Mare de Deu de la Mercè, Barcelona, Spain
[15]Hospital de Sant Joan Despí Moisès Broggi, Sant Joan Despí, Barcelona, Spain

Abstract: Huntington's disease (HD) is a neurodegenerative disorder which is primarily associated with striatal degeneration. However, the alterations in connectivity of this structure in HD have been underinvestigated. In this study, we analyzed the functional and structural connectivity of the left putamen, while participants performed a finger-tapping task. Using fMRI and DW-MRI, 30 HD gene

Contract grant sponsor: Ministerio de Economía y Competitividad (MINECO, Spanish Government). Instituto de Salud Carlos III, which is an agency of the MINECO, co-funded by European Regional Development Funds (ERDF); Contract grant numbers: CP13/00225; PI14/00834; Contract grant sponsor: FEDER funds; Contract grant sponsor: "La Caixa" Foundation

*Correspondence to: Estela Camara; Cognition and Brain Plasticity Unit, IDIBELL (Institut d'Investigació Biomèdica de Bellvitge), Feixa Larga S/N 08907, L'Hospitalet de Llobregat, Barcelona, Spain. E-mail: ecamara@ub.edu

Received for publication 21 March 2017; Revised 25 August 2017; Accepted 5 September 2017.

DOI: 10.1002/hbm.23813
Published online 8 October 2017 in Wiley Online Library (wileyonlinelibrary.com).

expansion carriers (HDGEC) and 29 healthy participants were scanned. Psychophysiological interaction analysis and DTI-based tractography were employed to examine functional and structural connectivity, respectively. Manifest HDGEC exhibited a reduced functional connectivity of the left putamen with the left and the right primary sensorimotor areas (SM1). Based on this result, the inhibitory functional connectivity between the left SM1 and the right SM1 was explored, appearing to be also decreased. In addition, the tract connecting these areas (motor corpus callosum), and the tract connecting the left putamen with the left SM1 appeared disrupted in HDGEC compared to controls. Significant correlations were found between measures of functional and structural connectivity of the motor corpus callosum, showing a coupling of both types of alterations in this tract. The observed reduction of functional and structural connectivity was associated with worse motor scores, which highlights the clinical relevance of these results. *Hum Brain Mapp 39:54–71, 2018*.

Key words: basal ganglia; Huntington's disease; interhemispheric connectivity; MRI; neurodegeneration; PPI; tractography

INTRODUCTION

Huntington's disease (HD) is a progressive neurodegenerative disease caused by the expansion of a cytosine-adenine–guanine (CAG) trinucleotide repeat within the *HTT* gene [MacDonald et al., 1993]. HD is characterized by a variety of motor, cognitive, and psychiatric symptoms that typically develop in adulthood years after the neurodegenerative process has begun [Paulsen et al., 2008]. Despite the multidimensional spectrum of HD, clinical diagnosis is based on the presence of unequivocal motor disability and most clinical trials use motor function as their primary endpoint [Bonelli and Hofmann, 2007].

Striatal atrophy is considered a hallmark of the disease, being observable between 15 and 20 years before the predicted onset [Aylward et al., 2004; Harris et al., 1999; Paulsen et al., 2008]. Striatal neuronal loss has been found to be correlated with CAG repeat length [Furtado et al., 1996; Kassubek et al., 2004; Penney et al., 1997; Rosas et al., 2001] and with motor dysfunction [Guo et al., 2012], suggesting an important role of this structure in the pathogenesis of HD.

Despite the fact that the striatum is of vital importance in HD, the functional connectivity of the putamen has been overlooked in the HD literature. Regarding the motor circuit, earlier neuroimaging studies focused on regional brain activity rather than connectivity [Bartenstein et al., 1997; Gavazzi et al., 2007; Klöppel et al., 2009].

Although regional brain activity studies offer important information about the effects of the disease on segregated brain areas, they only provide a partial account, as cognitive processes rely on the interaction between multiple brain regions that form complex networks [Rowe, 2010]. Regarding functional connectivity in the motor circuit, the effective connectivity during a tapping task has been studied in premanifest HD gene expansion carriers (HDGEC) using dynamic causal model (DCM) [Minkova et al., 2015; Scheller et al., 2013], showing a relationship between the connectivity patterns in this circuit and predicted years to clinical onset [Scheller et al., 2013].

Regarding structural connectivity of the motor circuit, diffusion measures of white matter connections between the putamen and the sensorimotor cortex have been found to be altered in manifest HDGC [Marrakchi-Kacem et al., 2013; Poudel et al., 2014] and to be correlated with speeded tapping performance [Poudel et al., 2014].

Although there is an extensive literature on structural and functional connectivity in HD separately, only recently studies have begun to examine how they interact with each other in HD [McColgan et al., 2017; Müller et al., 2016]. Elucidating the relationship between functional and structural connectivity in HD is crucial. This would shed light on the neurodegenerative processes that might be shared by other neurodegenerative diseases. Multimodal neuroimaging studies are thus of great interest to provide complementary structural and functional information from the same subject. Similarly, for a better understanding of the course of the disease, it is of vital importance to study the effects that alterations in both types of connectivity have on clinical symptoms.

How structural connectivity sustains and constrains functional connectivity is a question that remains unclear. Several studies have investigated this relationship in the healthy brain and have shown that although functional connectivity is generally constrained by structural connectivity, it can also exist between regions that are not structurally connected, possibly mediated by indirect structural connections [Adachi et al., 2012; Damoiseaux and Greicius, 2009; Park and Friston, 2013]. However, whether regions that are more strongly functionally connected also present stronger structural connections, has been less studied.

Recently, Müller et al. (2016) examined both structural and functional connectivity in the motor network in manifest HDGEC using deterministic tractography and resting-state functional magnetic resonance imaging (fMRI). In this study, the authors chose the thalamus and the primary somatosensory cortex (S1) as regions of interest to study the relation between structural and functional connectivity. However, they did not find a correlation

TABLE I. Mean and standard deviation of demographic and clinical information

	Controls $_A$	HD	Controls $_B$	manifest	Controls $_C$	Pre-HD
N	29	30	21	20	8	10
Gender (M/F)	14/15	10/20	11/10	10/10	3/5	0/10
Age	46.3 (10.4)	46.8 (12.4)	50.5 (8.7)	51.7 (10.4)	35.3 (5)	37.1 (10.5)
Education	12.7 (2.8)	11.7 (3)	12.3 (2.6)	10.7 (2.9)	13.6 (3.1)	13.7 (2)
CAG	-	44.3 (3.2)	-	44.1 (3.3)	-	44.7 (3.1)
CAP	-	102.7 (22.1)	-	111.5 (17.1)	-	85.2 (21.3)
TFC	-	12.2 (1.1)	-	11.8 (1.2)	-	12.9 (0.3)
UHDRS-motor	-	14.4 (12.1)	-	20.2 (10.4)	-	2.7 (4.1)
Years to onset	-	-	-	-	-	7.6 (10.8)

Control $_A$ is the whole group of controls matched for age and years of education with the HDGEC group. Control $_B$ is the subgroup of controls matched for age with manifest HDGEC. Control $_C$ is the subgroup of controls matched for age with pre HDGEC. Age and education are given in years. M, males; F, females; CAP, standardized CAG-Age product [Ross et al., 2014]; TFC, total functional capacity. Years to onset was calculated for each patient subtracting their age to the predicted age at onset [Langbehn et al., 2004].

between them, which is interpreted by the authors as a possible difference between individuals in the capability to adapt functional connectivity to try to compensate for the structural damage.

The aim of this study was to analyze whether there is a relationship between functional and structural connectivity alterations of the striato-cortical motor circuit in HDGEC and their correlation with motor disability. With this goal, we combined two neuroimaging modalities, task-based fMRI and diffusion tensor imaging (DTI) in the same subjects. We chose the putamen as a region of interest to investigate functional and structural connectivity in HD because of the importance of the striatum as a whole in HD and the role of the putamen in motor control in particular [Alexander et al., 1986; Lehéricy et al., 2006]. Furthermore, the putamen is one of the central hubs of the brain, which are structures that are highly connected, thus playing a central role in the overall network organization [Cole et al., 2010; Crossley et al., 2014; van den Heuvel and Sporns, 2011]. A change in its connectivity can therefore deeply affect the whole motor network. We hypothesized that altered functional connectivity of the putamen would be related with a decrease in structural connectivity.

METHODS

Participants

Thirty HDGEC participants (including 20 manifest and 10 premanifest HDGEC) and 29 healthy controls matched for age ($t(57) = -0.191$, $P = 0.849$) and years of education ($t(57) = -1.18$, $P = 0.242$) were scanned. Participants' demographics are detailed in Table I. Manifest HDGEC were defined as carriers of the genetic mutation with ≥ 36 repeats with a diagnostic confidence score (DCS) of 4 on the Unified Huntington's Disease Rating Scale (UHDRS) (Huntington Study Group, 1996), which corresponds to a confidence $\geq 99\%$ that the motor abnormalities are due to HD. According to criteria based on the Total Functional Capacity (TFC) score [Begeti et al., 2013], 17 of the manifest HDGEC were at the early stage of the disease (TFC: $M = 12.4$, $SD = 0.6$), whereas 4 of them were at moderate stage of the disease (TFC: $M = 9.8$, $SD = 0.4$). Premanifest HDGEC were defined as carriers of the genetic mutation with a $DCS < 4$ on the UHDRS. As a measure of the progression of HD pathology, we used the standardized CAG-Age Product (CAP) score, which is computed as: $CAP = 100 \times age \times (CAG - 35.5)/627$ [Ross et al., 2014].

None of the patients or controls reported previous history of traumatic brain injury or neurological disorder other than HD in the case of patients. All participants were right handed. Right-handedness was assessed using the Edinburgh handedness inventory [Oldfield, 1971]. All participants signed an informed consent to participate in this study, which was approved by the ethics committee of the Bellvitge Hospital. All the followed procedures were in accordance with the Helsinki Declaration of 1975.

Clinical Assessments

All HDGEC underwent the UHDRS evaluation, which was carried out by neurologists specialized in movement disorders. The UHDRS total motor score (range 0–124) was used as a measure of motor dysfunction, with higher scores indicating more severe motor disability. To describe the sample of HDGEC, the TFC score (range 0–13) was employed as a measure of independence in daily activities, which is used to determine the stage of the disease. In this case, higher scores indicate a higher degree of independence. Patients can be classified in early (TFC scores 11–13), moderate (TFC scores 7–10), or late (TFC scores 0–6) stages of the disease.

MRI Data Acquisition

MRI data were acquired through a 3 T whole-body MRI scanner (Siemens Magnetom Trio; Hospital Clínic, Barcelona), using a 32-channel phased array head coil. Structural

images comprised a conventional high-resolution 3D T1 image [magnetization-prepared rapid-acquisition gradient echo sequence (MPRAGE), 208 sagittal slices, repetition time (TR) = 1970 ms, echo time (TE) = 2.34 ms, inversion time (IT) = 1050 ms, flip angle = 9°, FOV = 25.6 cm, 1 mm isotropic voxel with no gap between slices].

For the motor task, each functional run consisted of 176 sequential whole-brain volumes. Each volume comprised 30 interleaved axial slices aligned to the plane intersecting the anterior and the posterior commissure with a 4 × 4 mm in-plane resolution, 4 mm slice thickness and no gap between slices, TR = 2000 ms, TE = 29 ms, flip angle = 80°, 64 × 64 acquisition matrix.

Diffusion-weighted MRI (DW-MRI) data were acquired using a diffusion tensor imaging sequence employing a dual spin-echo diffusion imaging sequence with GRAPPA (reduction factor of 4) cardiac gating, with TE = 92 ms. Images were measured using 2 mm isotropic voxels, no gap, 60 axial slices, and FOV = 23.6 cm. To obtain the diffusion tensors, diffusion was measured along 64 noncollinear directions, using a single b value of 1,500 s/mm^2 and interleaved with 9 nondiffusion $b = 0$ images. To avoid chemical shift artifacts, frequency-selective fat saturation was used to suppress fat signal.

Experimental Procedure

To examine the motor circuit in HDGEC, several neuroimaging studies have used sequential motor task paradigms [Bartenstein et al., 1997; Gavazzi et al., 2007; Klöppel et al., 2009; Weeks et al., 1997]. The details of those paradigms vary between studies but, in general, they consist on moving the fingers at the pace of an auditory tone. Unlike previous studies, we chose a self-paced sequential motor task to reduce the recruitment of the attentional networks [Witt and Stevens, 2013] and thus, have a more pure involvement of the motor circuit.

In our study, participants carried out a self-paced sequential tapping task with their right or left hand in alternated blocks with interleaved resting blocks while they were scanned. The run started with a rest block and each active block was followed by a resting block (rest, right, rest, left, and so on). Participants were instructed to move their index and middle fingers in an alternating fashion as quickly as possible. They were presented with blocks of 20 s of duration: 4 blocks of right-hand condition, 4 blocks left-hand condition, and 9 blocks of rest. A fixation cross was always present on the screen on a grey background. In the resting condition, the single fixation cross turned white. In the left and right hand conditions, a back-line drawing of a right hand (on the right side of a black fixation cross) or a left hand (on the left side of the fixation cross) was presented. The drawings of the hands had the index and middle fingers highlighted in white to indicate which fingers they should move (Fig. 2A). Before entering into the scanner, participants performed a brief training of the task on a laptop computer.

fMRI Regional Activity Analysis

Preprocessing and statistical analysis of fMRI data were performed using SPM8 software (http://www.fil.ion.ucl.ac.uk/spm/). After slice timing correction to minimize acquisition timing differences between slices, images were corrected for gradient inhomogeneities using fieldmap correction. Then, images were realigned and corrected for participant movement using ArtRepair software (http://www.cibsr.stanford.edu/tools/human-brain-project/artrepair-software.html), which is recommended for clinical populations that are prone to motion artefacts, as it is the case in HD. ArtRepair realigns functional images and after smoothing with a 7 mm full-width at half-maximum Gaussian kernel, it identifies and replaces outlier volumes, which are associated with excess of motion or spikes in the global signal, by a new volume corresponding to the interpolation of the two adjacent nonoutlier images. In particular, for each participant, outlier images were identified as those with more than 1.5% deviance from the mean but no more than two consecutive volumes were interpolated. No participant showed more than 7% of the volumes identified as outliers. Functional images were coregistered with the structural T1 image and normalized to the MNI template by using the Unified Segmentation Model approach [Ashburner and Friston, 2005]. During this step, spatial regularization (regularization: 0.02, discrete cosine transform warp frequency cutoff of 22) was adapted to account for striatal neurodegeneration and ventricle dilatation. Finally, images were spatially smoothed with a 4 mm isotropic Gaussian kernel.

Statistical analysis was carried out using a General Linear Model based on a least-square estimation (GLM) [Friston et al., 1995] in which right, left, and resting conditions were convolved with a box-car regressor waveform and with a canonical hemodynamic response function, and then included as regressors. Data were high-pass filtered (to a maximum of 1/128 Hz) and serial autocorrelations were estimated using an autoregressive model. Thus, a block-related design matrix was created including the conditions of interest (Right, Left, and Rest). After model estimation, the main effect of each condition was calculated and main contrasts were assessed: Right vs. Rest and Left vs. Rest.

For the fMRI analyses, we carried out separate analysis for manifest and premanifest HDGEC groups. As compensatory increases in brain activity can occur in premanifest HDGEC, including premanifest HDGEC together with manifest HDGEC could blur the differences with controls. We separated HDGEC in two groups, manifest ($n = 20$) and premanifest ($n = 10$) HDGEC. In order to compare the two groups with age-matched controls, we divided the controls in two subgroups, controls B ($n = 21$) and controls C ($n = 8$),

matched with manifest ($t(39) = -0.395$, $P = 0.695$) and pre-manifest HDGEC ($t(16) = -0.456$, $P = 0.654$), respectively.

First-level contrast images were entered into a second-level analysis using a one-sample t test including manifest HDGEC and controls together. To compare patients and controls, two-sample t tests were performed entering the corresponding (Right vs. Rest and Left vs. Rest) first-level contrasts. As manifest HDGEC were slower than healthy controls in the finger tapping task—and therefore performed fewer tappings per block—the mean number of tappings per block was introduced in the GLM as a confounding factor, to avoid finding differences in brain activity between manifest HDGEC and controls that could be explained by the difference in the tapping speed. Effects were considered significant at a whole-brain level if they exceeded a voxel-wise threshold of $P < 0.001$ ($k > 20$ voxels extent) and cluster-level family wise error (FWE) correction for multiple comparisons of $P < 0.05$. For the figures, a threshold of $P < 0.05$ FWE corrected for multiple comparisons across the whole-brain level was used. Anatomical and cytoarchitectonic areas were identified using the Automated Anatomical Labeling Atlas [Tzourio-Mazoyer et al., 2002] included in the xjView toolbox (http://www.alivelearn.net/xjview8/).

Brain Connectivity Analysis

A psychophysiological interaction (PPI) analysis [Friston et al., 1997] was performed to examine the functional connectivity between the putamen and the rest of the brain during the finger tapping task. Specifically, in this study, we were interested in how the physiological connectivity between the left putamen and the rest of the brain varied with the movement of the right hand compared to rest. We chose the left putamen because the left striatum has been shown to be more affected than the right putamen in HDGEC [Jenkins et al., 1998; Paulsen et al., 2004; Rosas et al., 2001].

We used the fMRI results of the Right versus Rest contrast as a localizer to obtain the peak coordinate of the left putamen in each participant individually. The threshold was set to $P < 0.05$ uncorrected. In those participants in which no activation was found in the left putamen at this threshold (a total of two HDGEC and three controls), this was decreased as much as necessary. As the clusters extended beyond the left putamen in many cases, we included a mask of the left putamen in each subject individually to restrict the search of the peak coordinate to the left putamen. A 4-mm-radius sphere seed was defined around the peak coordinate in each case.

For each participant, we extracted the first eigenvariate of the BOLD time series from all the voxels within the left putamen sphere. Then, the canonical hemodynamic response function (HRF) was deconvolved to derive the neural signal of the source region. The PPI regressor was calculated as the product of the deconvolved time series and a vector coding for the psychological variable (1 for right hand, −1 for rest, and 0 for left hand). The result of this product was then reconvolved with the canonical HRF to create the final PPI regressor. The PPI model for each subject included as regressors the psychological (Right vs. Rest), the physiological (the left putamen signal), and the derived psychophysiological variables.

Individual first-level analyses were carried out and main contrasts were estimated to test the effects of the PPI regressor. The computed PPI contrast images were entered into a second-level random effects analysis (two-sample t test), where the mean number of tappings per block was introduced as a regressor of no interest to control for the differences in speed between manifest HDGEC and healthy controls when comparing the functional connectivity of both groups.

Results were considered significant at a whole-brain level if they exceeded a voxel-wise threshold of $P < 0.001$ ($k > 20$ voxels extent) and cluster-level family wise error (FWE) correction for multiple comparisons of $P < 0.05$. For the figures, a threshold of $P < 0.05$ FWE corrected for multiple comparisons across the whole-brain level was used.

As a result of the findings of this analysis, PPI beta values were extracted individually in the peak coordinate of the left SM1 and the right SM1 (Fig. 1). These were chosen as the two areas were found to be functionally connected differently in manifest patients and controls. This measure was extracted to acquire a measure of functional connectivity between the left putamen and the left and right SM1.

To further investigate the interplay between the right and the left SM1 and obtain the strength of functional connectivity between them, a second PPI analysis was run. With that purpose, the left and the right SM1 were functionally localized by using the group mean peak coordinates, for patients and controls separately, in the contrasts Right versus Rest and Left versus Rest, respectively. A 6-mm-radius sphere centered at the peak coordinate was then taken as a seed region for the PPI analysis (Fig. 1). The PPI values from this analysis were extracted for each subject in the peak coordinate of the right SM1 to obtain a measure of functional connectivity between the left and the right SM1.

DW-MRI Tractography Analysis

Preprocessing of DTI data

First, brain extraction was performed using the FSL Brain Extractor Tool [Smith, 2002]. Head motion and eddy-current correction were then performed using the FMRIB's Diffusion Toolbox (FDT) in FMRIB's Software Library (FSL, http://www.fmrib.ox.ac.uk/fsl/fdt) and the gradient matrix was rotated (Leemans and Jones, 2009). The diffusion tensor was then reconstructed using Diffusion Toolkit's least-squares estimation algorithm for each voxel provided in Diffusion Toolkit (http://www.trackvis.org/dtk) and its corresponding eigenvalues and eigenvectors were extracted to calculate the fractional anisotropy (FA), axial diffusivity

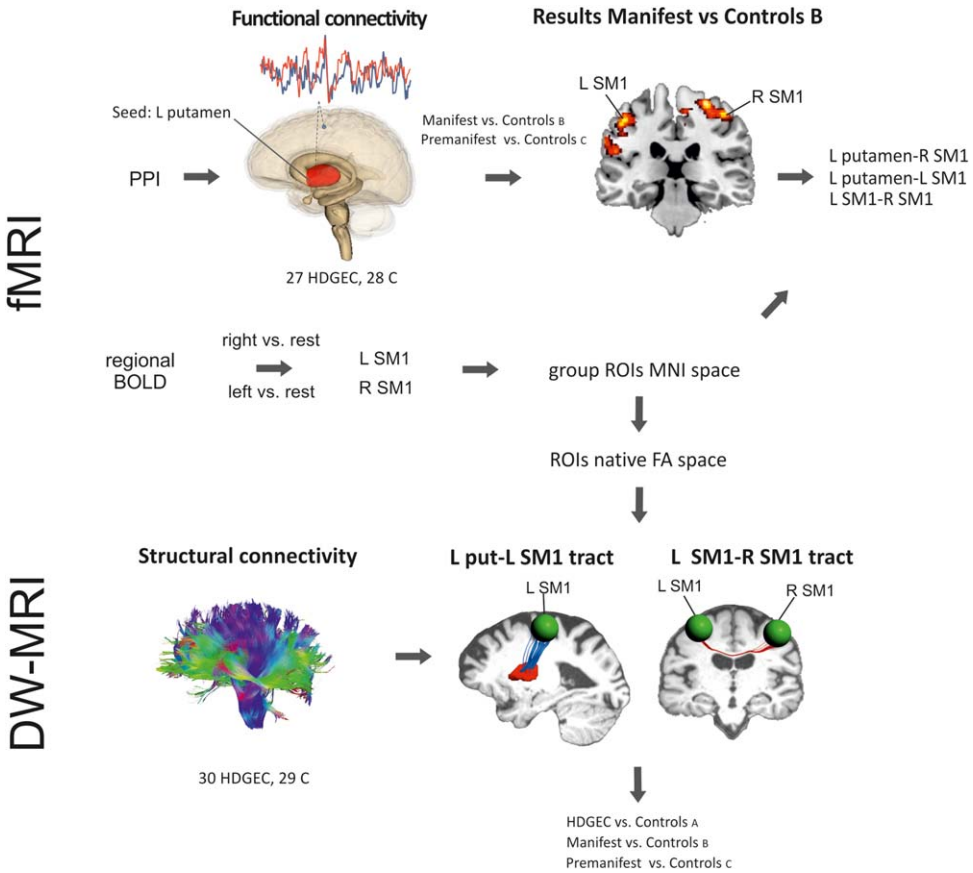

Figure 1.

Scheme of methods, showing the relationship between fMRI and tractography analyses regarding the election of ROIs. The number of participants included in each modality and the groups compared are also indicated.

(AD), radial diffusivity (RD), and apparent diffusion coefficient (ADC) maps.

Fiber orientation distributions (FOD) were reconstructed using a spherical deconvolution approach based on the damped version of the Richardson–Lucy algorithm [Dell'Acqua et al., 2010] implemented in StarTrack software (http://www.natbrainlab.co.uk). We first visualized FOD fields in selected a priori fiber-crossing regions (Splenium of the corpus callosum and corona radiata). We then selected a combination of SD parameters that nicely resolved crossing and, at the same time, avoided spurious peaks in GM or CSF (a fixed fiber response corresponding to a shape factor of $\alpha = 2 \times 10^{-3}$ mm^2/s; 200 algorithm iterations, regularization threshold $\eta = 0.04$, and regularization geometric parameter $v = 8$ (see Dell'Acqua et al. [2010] for full details of these parameters).

Whole-brain tractography was then performed using a *b*-spline interpolation of the diffusion tensor field and Euler integration to propagate streamlines following the directions of the principal eigenvector with a step size of 0.5 mm [Basser et al., 2000]. Tractography was started in all brain voxels with FA > 0.2 and was stopped when FA < 0.2 or when the angle between two consecutive tractography steps was larger than 35°. Finally, tractography data and diffusion tensor maps were exported into Trackvis (http://www.trackvis.org) for manual dissection of the tracts.

Tractography dissections

To investigate the link between functional and structural connectivity, we virtually dissected two different motor tracts: the left putamen–left SM1 tract and the motor corpus callosum (CC). Individual tractography dissections were performed in native space using the two regions of interest (ROIs) approach, which permits the reconstruction of the fibers that connect these regions.

For the virtual dissection of the left putamen–left SM1 tract, the left putamen and the left SM1 were defined as ROIs, whereas the motor CC was dissected using the left and the right SM1 as ROIs.

The left putamen was defined by using automated segmentation with the FreeSurfer 5.1.0 software [Fischl et al., 2002]. Then, this ROI was registered to the individual native diffusion space using the FSL FLIRT [Jenkinson and Smith, 2001] and FNIRT [Andersson et al., 2007] modules after normalizing both the structural T1 images and FA maps. For the left and right SM1 ROI, 16-mm-radius spheres were drawn using TrackVis. The center of the spheres was originally set to the mean peak coordinate in the contrast Right versus Rest for the left SM1 and the contrast Left versus Rest for the right SM1 for both groups (manifest HDGEC and healthy controls) separately. The peak coordinate was defined in the MNI space and was wrapped back to the individual native diffusion space using the inverse matrix transformation obtained using FSL FLIRT and FNIRT modules after normalizing the native FA maps (Fig. 1). In the native diffusion space, the spheres were slightly moved around the coordinate if necessary to correctly segment the tract of interest. The fibers of the dissected tracts were constrained to end within the putamen but in the case of the left and right SM1 ROIs, they were allowed to freely project until they reached the cortex.

Diffusion measures (FA, AD, RD, and ADC) were extracted and averaged along the entire delineated tracts. For the analyses comparing the diffusion indices of the white-matter tracts between patients and controls, both manifest and premanifest HDGEC were included in a single group, since reduced structural connectivity has been shown already in premanifest HDGEC [Klöppel et al., 2008; Matsui et al., 2015; Di Paola et al., 2012, 2014; Phillips et al., 2015, 2016; Poudel et al., 2014, 2015; Reading et al., 2005; Rosas et al., 2006, 2010; Tabrizi et al., 2009; Thieben et al., 2002]. However, to have a more detailed information of the structural connectivity pattern at different stages of the disease progression, we also performed the same analyses dividing manifest and premanifest HDGEC. Two-sample t tests were carried out to compare the diffusion metrics of each tract in HDGEC and controls and the corresponding Cohen's d was calculated as an effect size estimate.

Correlation Analyses

Regarding the relationship between clinical measures with both functional and structural connectivity alterations, Pearson's correlation analyses were performed between UHDRS motor and CAP scores and both the PPI parameter estimates and the diffusion indices (FA, RD, AD, and ADC) of the two tracts investigated. Results were corrected for multiple comparisons by controlling the false discovery rate (FDR) at $P < 0.05$ using the Benjami–Hochberg procedure, taking into account the number of PPI estimates and the number of tracts.

Second, to investigate the relationship between functional and structural connectivity, Pearson's correlation analyses were carried out between the left putamen–left SM1 and the left SM1–right SM1 PPI parameter estimates and the diffusion indices of the white-matter tracts connecting these regions, namely, the left putamen–left SM1 tract and the motor CC.

Both manifest and premanifest HDGEC were included together in the correlation analyses to have a large range of values that would allow studying the disease as a continuum. Furthermore, in the case of the relationship between functional and structural connectivity, one of the main goals of the study, separate correlation analyses were carried out including only manifest HDGEC, which was the group that showed significant differences in functional and structural connectivity compared to controls.

RESULTS

Behavioral Results

Two manifest HDGEC and one control did not perform the finger tapping task correctly inside the scanner. In one case, the button box was displaced during the scanning during the task and the participant pressed the wrong buttons. In the other two cases, participants did not release the button corresponding to the middle finger, keeping it constantly pressed during the execution of the tapping task. These subjects were not included either in the performance or in the fMRI analyses, resulting in a total of 27 HDGEC and 28 controls. Behavioral performance was evaluated using the mean number of tappings per block for the right and the left hand separately. Two-sample t tests were used to compare performance between HDGEC and controls in the tapping task and. Cohen's d was calculated as an estimate of the effect size [Cohen, 1977]. The mean number of tappings per block was significantly lower in manifest HDGEC (right hand: $M = 42.5$, $SD = 14.6$; left hand: $M = 35.2$, $SD = 14.2$) than in controls (right hand: $M = 79.7$, $SD = 30.6$; left hand: $M = 66.2$, $SD = 20.2$) both for the right hand ($t(26.042) = 4.763$, $P < 0.001$, $d = 1.85$) and the left hand conditions ($t(35) = 5.374$, $P < 0.001$, $d = 1.81$). In the case of the premanifest HDGEC, the mean number of tappings (right hand: $M = 64.3$, $SD = 27.4$; left hand: $M = 58.2$, $SD = 28.3$) was not significantly different compared with the matched controls (right hand: $M = 95.7$, $SD = 39.3$; left hand: $M = 85.9$, $SD = 28.1$) for either the right hand ($t(15) = 1.932$, $P = 0.072$, $d = 1.01$) or the left hand ($t(15) = 1.830$, $P = 0.087$, $d = 0.95$).

Regional Brain Activity Results

We first carried out a regional brain activity conjunction analysis to identify the motor network engaged during the fMRI finger tapping task. Whole-brain analysis revealed activation of contralateral primary sensorimotor areas (SM1) (precentral and postcentral gyri), the supplementary motor area (SMA), and the ipsilateral cerebellum, and visual areas (Fig. 2B and Table II). Moreover, using a less conservative multiple comparisons correction ($P < 0.05$ FDR corrected at voxel level), activations in subcortical

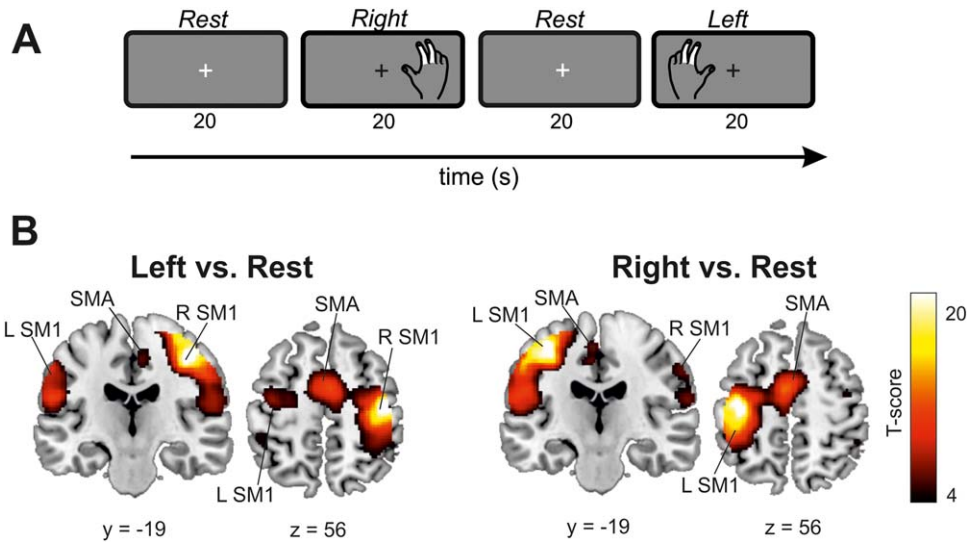

Figure 2.

Schematic representation of the fMRI block design in the finger-taping task and overall pattern of activations in the task. A) Schematic representation of the finger tapping task. B) Regional brain activity results of the main contrast of interest Left vs Rest (left panel) and Right vs Rest (right panel) ($P < 0.05$ FWE-corrected at voxel level, cluster size > 20). The numbers indicate the coordinate of the slice in MNI space. L SM1: left primary sensorimotor area. R SM1: right primary sensorimotor area. SMA: supplementary motor area.

structures such as the contralateral putamen (left putamen: $x = -28$, $y = -12$, $z = 0$; right putamen: $x = 20$, $y = 6$, $z = 2$) and thalamus (left thalamus: $x = -17$, $y = -17$, $z = 15$; right thalamus $x = 14$, $y = -22$, $y = 0$) were observed.

Although manifest patients presented a reduced level of activity in this network compared with matched controls, this difference was not statistically significant when correcting for multiple comparisons. No significant difference in the level of brain activity was found when comparing premanifest HDGEC with the corresponding matched control group.

Pyschophysiological Interaction Results

A PPI analysis was then carried out taking the left putamen as a seed region to study its functional connectivity

TABLE II. Regional activity conjunction analyses ($P < 0.05$ FWE-corrected at cluster level, $P < 0.001$ uncorrected voxel level, cluster extent >20 voxels)

		MNI coordinates					
Anatomical area	Side	*x*	*y*	*z*	Cluster size (voxels)	*T* max	*P* (FWE-corr cluster)
Right vs. Rest							
Precentral gyrus	L	−38	−14	58	10,305	22.89	<0.001
SMA	L	−4	−4	54		12.62	<0.001
Postcentral gyrus	L	−60	−18	20		11.25	<0.001
Cerebellum	R	22	−50	−24	2,647	11.42	<0.001
MOG	L	−40	−72	−14	1,704	11.04	<0.001
Postcentral gyrus	R	60	−34	26	1,443	9.11	<0.001
Precentral gyrus	R	56	10	14	558	6.63	0.003
Left vs. Rest							
Precentral gyrus	R	40	−18	52	14,084	26.49	<0.001
SMA	R	4	−2	58		11.88	<0.001
Cerebellum	L	−22	−54	−24	1,244	9.23	<0.001
MOG	R	34	−86	−4	986	7.68	<0.001
MOG	L	−26	−90	−2	670	6.57	0.001

SMA, supplementary motor area; MOG, middle occipital gyrus.

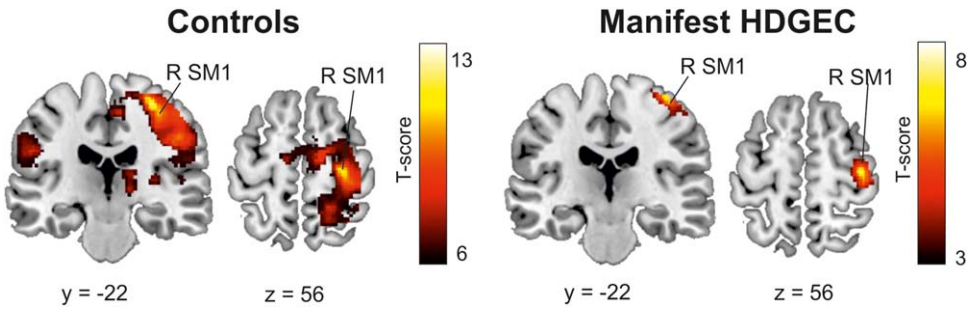

Figure 3.
Functional connectivity results taking the left putamen as a seed region in controls and manifest HDGEC ($P < 0.05$ FWE-corrected at voxel level, cluster extent > 20). The numbers indicate the coordinate of the slice in MNI space. R SM1: right primary sensorimotor area.

with the rest of the brain during the movement of the right hand compared with rest.

Within-group functional connectivity patterns of the manifest HDGEC and the control groups are shown in Figure 3 and Table III. In controls, the right SM1 and the right cerebellum were negatively connected with the left putamen, whereas in manifest HDGEC, only the right SM1 showed a significant negative connectivity with the left putamen. Neither the control nor the patient group showed regions that were significantly positively connected with the left putamen during Right versus Rest.

The comparison between manifest HDGEC and controls revealed a reduction in the strength of connectivity between the left putamen and the left and right SM1 in HDGEC (Fig. 4 and Table III). No significant difference was found in the connectivity of the left putamen between premanifest HDGEC participants and the corresponding matched controls. Hence, in the second follow-up PPI analysis, we focused only in the manifest group.

For the second PPI analysis, the left SM1 was taken as a seed region and the PPI beta values of the Right versus Rest contrast were extracted from the right SM1 ROI. Both manifest HDGEC and controls presented negative functional connectivity between the left and the right SM1. When we compared the PPI values of functional connectivity between left SM1 and right SM1 in manifest HDGEC and controls, we found a significant reduction in the strength of connectivity in patients ($t(51) = 2.869$, $P = 0.006$, $d = 0.80$).

Relationship Between Altered Functional Connectivity and Motor Disability

First, to study whether the abnormalities found in functional connectivity in manifest HDGEC were related with motor disability, Pearson's correlation analyses were carried out between the UHDRS motor scores and the PPI parameter estimates between left putamen–left SM1, left putamen–right SM1, and left SM1–right SM1. More severe motor disability (higher UHDRS motor score) was associated with reduced strength of the functional connectivity of the putamen: left putamen–left SM1 ($r = 0.51$, $P = 0.007$) and left putamen–right SM1 ($r = 0.55$, $P = 0.005$) but also with the interhemispheric connectivity between left and right SM1 ($r = 0.56$, $P = 0.005$). In contrast, the correlation between functional connectivity and disease burden, measured by the CAP score, indicated that higher disease burden was associated only with reduced strength of

TABLE III. Whole-brain functional connectivity analyses with seed in the left putamen ($P < 0.05$ FWE-corrected at cluster level, $P < 0.001$ uncorrected voxel level, cluster extent >20 voxels)

		MNI coordinates					
Anatomical area	Side	*x*	*y*	*z*	Cluster size (voxels)	*T* max	*P* (FWE-corr cluster)
Controls							
Precentral gyrus	R	28	−20	60	48,631	13.14	<0.001
Postcentral gyrus	R	40	−30	56		10.29	
Cerebellum	R	16	−32	−24	275	8.12	0.007
Manifest HD							
Precentral gyrus	R	38	−18	62	380	7.27	0.003
Manifest HD vs. controls							
Postcentral gyrus	L	−44	−38	50	822	5.22	<0.001
Postcentral gyrus	R	28	−28	64	996	5.04	<0.001

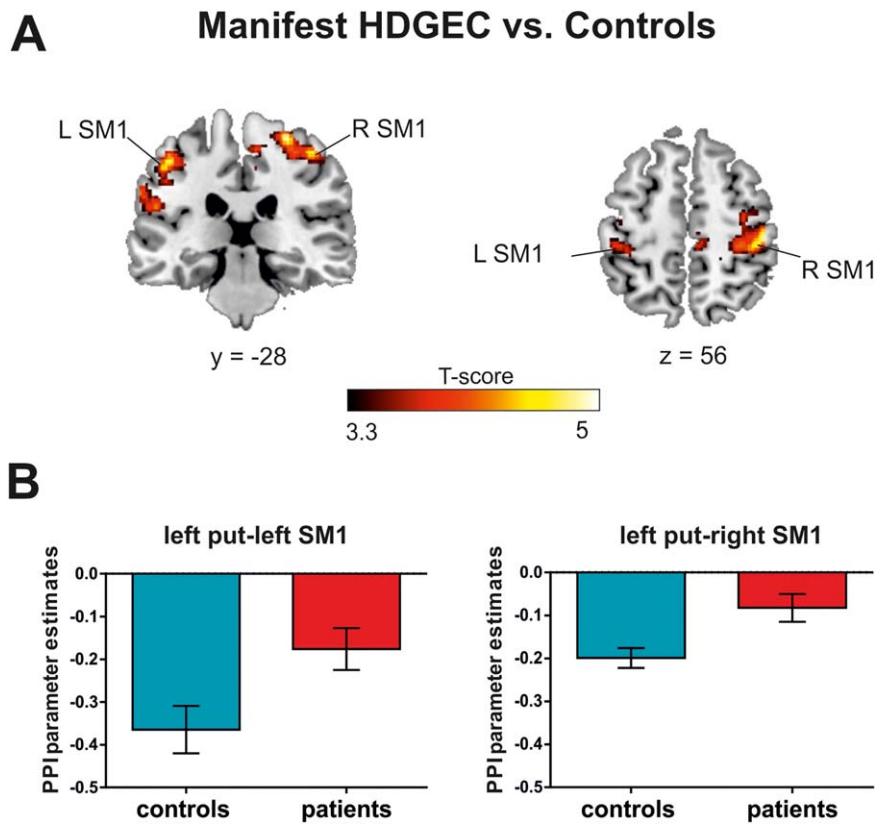

Figure 4.

A) Functional connectivity results: between-group differences ($P < 0.05$ FWE-corrected at voxel level, cluster extent > 20). The numbers indicate the coordinate of the slice in MNI space. L SM1: left primary sensorimotor area. R SM1: right primary sensorimotor area. B) PPI parameter estimates of the functional connectivity analyses between the left putamen and the left SM1 (left panel) and between the left putamen and the right SM1 (right panel) in controls and manifest HDGEC.

functional connectivity of the putamen: left putamen–left SM1 ($r = 0.51$, $P = 0.018$) and left putamen–right SM1 ($r = 0.46$, $P = 0.026$). In this case, no significant correlation was found with left SM1–right SM1 ($r = 0.23$, $P = 0.248$).

Tractography Results

Two tracts were thus chosen to examine whether the observed abnormal functional connectivity was related to white-matter damage between the areas showing altered functional connectivity in the PPI analysis. First, the intrahemispheric tract between the left putamen and the left SM1 was segmented in every subject, as the functional coupling between these two areas was found to be significantly altered in manifest HDGEC. Figure 5A shows an example of the segmented left putamen-left SM1 tract in a control and a manifest HDGEC projected into their native T1 image.

As a whole, the group of HDGEC individuals showed reduced structural connectivity in the left putamen–left SM1 tract. They had higher average ADC, AD, and RD values compared with controls. However, average FA values were not significantly different (see Table IV for details). A post-hoc analysis indicated that this result was driven specifically by the manifest HDGEC group who had significantly higher average ADC ($P = 0.006$), AD ($P < 0.001$), and RD ($P = 0.027$) values compared to controls. This altered structural connectivity was not present in the premanifest group compared to their matched controls.

The second tract that was segmented was the motor CC, which was defined as the part of the CC that connected the left and the right SM1 (Fig. 5B). This tract was chosen since the reduced functional coupling between the left putamen and the right SM1 in manifest patients indicated that some interhemispheric tract could be damaged. Previous studies using transcranial magnetic stimulation (TMS) (for a review, see Beaulé et al. [2012]) and fMRI [Allison et al., 2000; Aramaki et al., 2006; Grefkes et al., 2008] have shown that interhemispheric inhibition of motor cortices

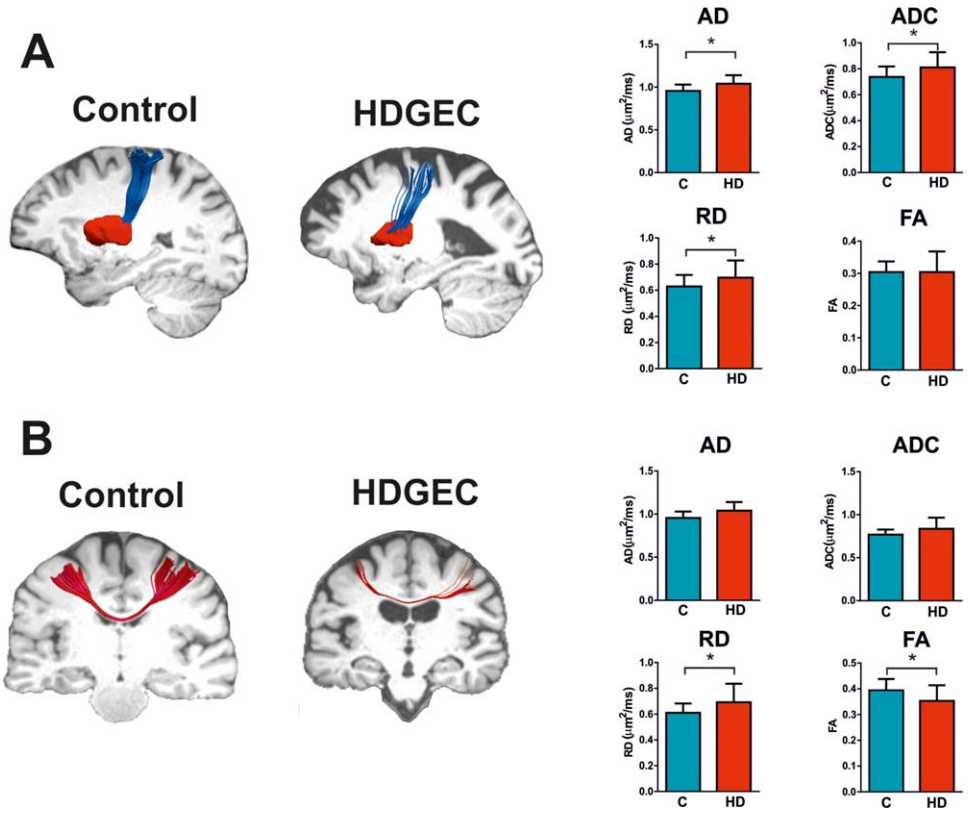

Figure 5.

Tracts segmented and diffusion indices. A) Sagittal views of the left putamen-left SM1 tract projected into the native T1 image of a control and a HDGEC and the corresponding diffusivity indices in controls and HDGEC. B) Coronal views of the motor corpus callosum (CC) tract and the corresponding diffusivity indices in controls and HDGEC. Bar plots show the mean diffusion indices values and error bars represent the standard deviation of diffusion indices. AD: axial diffusivity. ADC: apparent diffusion coefficient. RD: radial diffusivity. FA: fractional anisotropy.

via transcallosal fibers facilitates unilateral movements to prevent mirror movements in the unused hand. We hypothesized that the observed reduced functional connectivity between left putamen and right SM1 in manifest patients could be due to both left putamen–left SM1 and left SM1–right SM1 reduced structural connectivity, and therefore the left SM1–right SM1 connection (motor CC) was also investigated.

Importantly, due to the presence of marked atrophy, the motor CC could not be segmented in 12 out of the 30 patients in contrast to the only three controls (two of them were the oldest controls of the group, with 60 and 69 years of age) where this occurred. For those subjects in which it was possible to segment the motor CC, the diffusion values were extracted. Given the relative small number of data-points for the diffusion measures, we explored the relationship with motor disability by dividing the patients in two groups with high and low structural connectivity. In order to obtain the two groups, the median number of streamlines was calculated (median = 12.5) and three groups of 10 participants each were formed. The 10 highest values above the median group (M = 119.8, SD = 72.6) were included in the high structural connectivity group and the 10 lowest values (all of them with cero streamlines) in the low connectivity group. Individuals with intermediate values (M = 10.9, SD = 7.2) were not included to obtain more differentiated groups. The structural connectivity of the motor CC was found to be reduced in HDGEC, with significantly decreased mean values of FA and significantly increased mean values of RD compared with healthy controls. Although the increased mean values of ADC and AD in HDGEC compared to controls were not significant the effect size of the increase of ADC reveals a medium effect (see Table IV for details).

As we observed with the previous track, when taking only manifest HDGEC alone, the average ADC ($P = 0.039$) and RD ($P = 0.040$) values were found to be higher compared to the subgroup of matched controls. In contrast, premanifest HDGEC did not show significant differences in the structural connectivity of the motor CC compared with controls.

TABLE IV. Mean and standard deviation of the tract-based diffusion indices, statistics of the two-sample *t* test and the effect sizes of the comparison between HDGEC and controls

	ADC	RD	AD	FA
Left putamen–left SM1 tract				
Controls	0.74 (0.08)	0.63 (0.09)	0.10 (0.07)	0.30 (0.03)
HD	0.81 (0.12)	0.70 (0.13)	1.04 (0.10)	0.30 (0.06)
Controls vs. HD	$t(49.65) = -2.727$	$t(48.79) = -2.253$	$t(56) = -3.625$	$t(42.05) = 0.41$
	$P = 0.009$*	$P = 0.029$*	$P = 0.001$*	$P = 0.968$
	$d = 0.77$	$d = 0.65$	$d = 0.97$	$d = 0.01$
Motor corpus callosum tract				
Controls	0.77 (0.06)	0.61 (0.07)	1.09 (0.05)	0.39 (0.04)
HD	0.84 (0.13)	0.69 (0.14)	1.12 (0.12)	0.35 (0.06)
Controls vs. HD	$t(20.41) = 2.025$	$t(21.40) = 2.189$	$t(21.09) = 1.296$	$t(41) = -2.601$
	$P = 0.056$	$P = 0.040$*	$P = 0.209$	$P = 0.013$*
	$d = 0.90$	$d = 0.95$	$d = 0.10$	$d = 0.81$

Mean apparent diffusion coefficient (ADC), radial diffusivity (RD), and axial diffusivity (AD) are in units of $\mu m^2/ms$. Fractional anisotropy (FA) is dimensionless.

Relationship Between Altered Structural Connectivity and Motor Disability

To study whether reduced structural connectivity was associated with motor disability, Pearson's correlation analyses were performed between the diffusion values (FA, RD, AD, and ADC) of the two tracts studied and UHDRS motor scores. Whereas AD, ADC, and RD in the left putamen–left SM1 tract were all significantly correlated with UHDRS motor score (AD: $r = 0.69$, $P < 0.001$; ADC: $r = 0.59$, $P = 0.002$; RD: $r = 0.54$, $P = 0.002$), only AD reached significance in the case of the moor CC tract (AD: $r = 0.48$, $P = 0.045$; ADC: $r = 0.45$, $P = 0.062$; RD: $r = 0.43$, $P = 0.077$). The correlation coefficients showed nevertheless a moderate effect size for all of the diffusion measures except FA. FA was not significantly associated with motor disability in either the left putamen–left SM1 tract ($r = -0.38$, $P = 0.08$) or the motor CC tract (FA: $r = -0.25$, $P = 0.319$). In both tracts, only AD significantly correlated with disease burden, as measured by the CAP score (left putamen–left SM1 tract: $r = 0.47$, $P = 0.018$; motor CC tract: $r = 0.49$, $P = 0.040$).

We then divided the patients in two groups according to the number of streamlines in the motor CC—low and high structural connectivity—and the UHDRS motor score of the two groups was compared. Patients with low structural connectivity in the motor CC showed significantly ($t(18) = 2.430$, $P = 0.026$) higher UHDRS motor scores (M= 14, SD = 7.36) than patients with high structural connectivity in this tract (M= 6.10, SD = 7.17).

Relationship Between Functional and Structural Connectivity

After segmenting the left putamen–left SM1 tract and the motor CC, we investigated the relationship between the structural connectivity of these tracts and the functional connectivity between the regions connected by them. For this, Pearson's correlation analyses were carried out. In the case of the left putamen-left SM1 tract, no significant correlation was observed between any of the diffusion measures and the PPI values in either HDGEC (FA: $r = 0.17$, $P = 0.391$; ADC: $r = 0.07$, $P = 0.719$; AD: $r = 0.21$, $P = 0.298$; RD: $r = 0.01$, $P = 0.949$) or controls (FA: $r = -0.29$, $P = 0.156$; ADC: $r = 0.01$, $P = 0.971$; AD: $r = -0.09$, $P = 0.654$; RD: $r = 0.06$, $P = 0.788$). These correlations remained nonsignificant when taking the manifest HDGEC group alone.

In the case of the motor CC tract, interestingly, we found a significant correlation between functional and structural connectivity in HDGEC. Diffusion values of ADC ($r = -0.54$, P =.025), AD ($r = 0.51$, $P = 0.038$) and RD ($r = 0.54$, $P = 0.025$) but not FA ($r = -0.44$, $P = 0.075$) of the motor CC were significantly correlated with left SM1–right SM1 functional connectivity in HDGEC (Fig. 6). In contrast, no diffusion measure was significantly correlated with functional connectivity in controls (FA: r =.03, $P = 0.872$; ADC: $r = 0.03$, $P = 0.872$; AD: $r = 0.07$, $P = 0.732$; RD: $r = 0.01$, $P = 0.957$). Thus, in HDGEC, a decrease in the strength of interhemispheric functional connectivity between left and right SM1 was associated with decreased structural connectivity between these two areas.

When taking the manifest HDGEC group alone, the correlation between functional and structural connectivity in the motor CC tract remained significant. Specifically, average diffusion values of FA ($r = -0.75$, $P = 0.019$), ADC ($r = 0.71$, $P = 0.03$) and RD (r =.74, $P = 0.023$) correlated significantly with left SM1–right SM1 functional connectivity, whereas AD did not significantly correlate ($r = 0.59$, $P = 0.092$).

DISCUSSION

In this study, we examined changes in the functional and structural connectivity of the striato-cortical motor

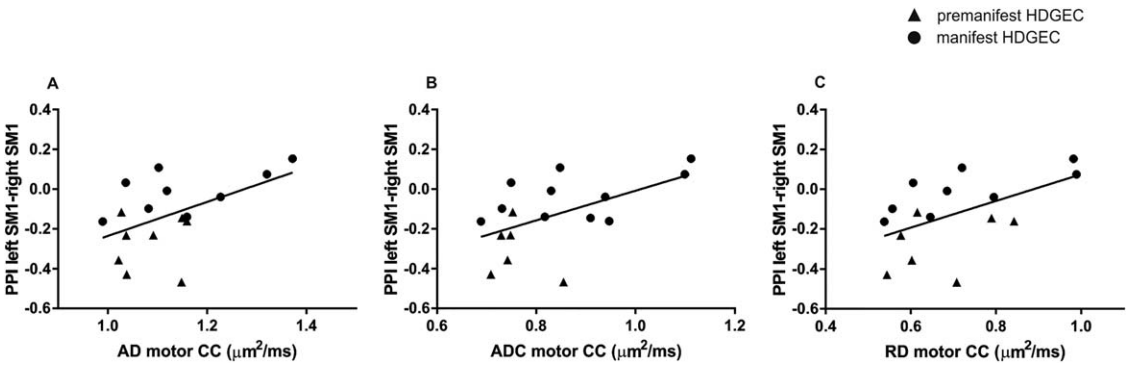

Figure 6.

Scatter plots of the correlations between the PPI parameter estimates of the functional connectivity analyses between the regions connected by the motor corpus callosum and the diffusion indices of this tract. A) AD: axial diffusivity. B) ADC: apparent diffusion coefficient. C) RD: radial diffusivity.

circuit in HD, the relationship between the two kinds of connectivity and their association with motor disability.

We obtained three main results. First, during the movement of the right hand, the strength of negative functional connectivity between the left putamen and both left and right SM1 was decreased in manifest HDGEC compared to healthy controls. Similarly, the negative functional connectivity between the left and the right SM1 was decreased in manifest HDGEC. Furthermore, the decrease of functional connectivity in the three connections studied was associated with worse motor scores. Disease burden significantly correlated with left putamen functional connectivity with both ipsilateral and contralateral SM1 but not with interhemispheric connectivity between left and right SM1. Despite the fact that the premanifest group was on average at <10 years from estimated disease onset, differences in functional connectivity compared to controls were not observed in this group. However, it is worth pointing out the variability in years to onset between our sample of premanifest HDGEC as well as the small size of the group ($n = 10$), both factors being possible contributors to the lack of differences with controls.

Second, the two white-matter tracts explored—the intrahemispheric left putamen–left SM1 tract and the interhemispheric motor CC—were altered in HDGEC. In addition, less integrity in both tracts was associated with more severe motor disability and higher disease burden. Third, only the motor CC showed a significant correlation between the structural connectivity of the tract and the functional connectivity between the regions connected by it. A reduction in structural connectivity was associated with a decrease in the strength of functional connectivity.

More specifically, both in patients and controls, the left putamen PPI analysis showed a negative functional connectivity with the right-hemisphere cortical motor areas during the movement of the right hand. This negative functional connectivity with the motor circuit of the nonmoving hand is consistent with previous studies that have shown that the execution of unilateral motor movements requires transcallosal interhemispheric inhibition of the ipsilateral M1 by the contralateral M1 to suppress motor output of the passive hand [Allison et al., 2000; Aramaki et al., 2006; Ferbert et al., 1992; Fling et al., 2013; Grefkes et al., 2008; Leocani et al., 2000; Liepert et al., 2001]. As the areas showing negative connectivity with the left putamen are part of the right motor circuit, we interpret this pattern as a consequence of the inhibition of these areas by the left SM1 during the movement of the right hand.

Although both groups showed a similar functional connectivity pattern between the left putamen and sensorimotor areas, manifest HDGEC showed a significant reduction in the strength of the connectivity between the putamen and the left and right SM1 compared with healthy controls. Regarding the interhemispheric connectivity between the left putamen and the right SM1, we hypothesized that the decreased strength of connectivity observed in manifest HDGEC could be due to a reduced transcallosal inhibition of the right motor circuit by the left SM1. As a consequence, the right SM1 would be deactivated to a lesser extent in patients compared to controls, thus resulting in a damped negative connectivity between the left putamen and the right SM1.

To investigate this hypothesis, we carried out a second PPI analysis taking the left SM1 as a seed region and extracted the connectivity values from an ROI region in the right SM1. Both controls and manifest HDGEC showed a negative connectivity between the left and the right SM1, which we again interpret as a inhibitory connectivity that suppress right SM1 activity to perform unilateral movements. As we had hypothesized, manifest HDGEC showed a significant reduction in the strength of functional connectivity compared to healthy controls. This result is consistent with previous studies that have shown impaired interhemispheric processing [Bocci et al., 2016] and reduced inhibition

of the ipsilateral hemisphere during hand movement execution [Beste et al., 2009] in manifest HDGEC using transcranial and event related potentials, respectively.

Therefore, the results from the second PPI analysis suggest that the altered functional connectivity between the left putamen and the right SM1 that was found in the first PPI analysis could be due to altered intrahemispheric connectivity between the left putamen and the left SM1 and abnormal interhemispheric connectivity between the left SM1 and the right SM1. In all three cases (left putamen–left SM1, left putamen–right SM1, and left SM1–right SM1), a reduced strength in functional connectivity values was significantly associated with more severe motor disability.

Given that the putamen is one of the first regions to be affected in HD, it is possible that the abnormal function of the left putamen and its altered functional connectivity with the sensorimotor cortex affects the function of the sensorimotor cortex itself. This dysfunction in turn results in an altered interhemispheric functional connectivity between the left and right motor cortices in HDGEC. The putamen is one of the main hubs of the brain [Cole et al., 2010; Crossley et al., 2014; van den Heuvel and Sporns, 2011]. A lesion on a hub has a disproportionate impact on the network's functioning, which gives brain hubs an important role in brain disorders [Crossley et al., 2014]. Therefore, early malfunction of the putamen in HD can alter its functional connectivity with other regions, thus spreading the damage to other brain areas that are directly and indirectly connected with it, as we find in our results.

To further explore the damage in the motor circuit in HD and to investigate whether structural connectivity was also reduced, we next studied the microstructural organization of the white matter pathways that connected the areas whose functional connectivity was found to be significant altered in manifest HDGEC. Indeed, the structural connectivity of both the left putamen–left SM1 and the motor CC tracts was also reduced in HDGEC. This effect was driven by the manifest HDGEC group, as connectivity measures were comparable in premanifest HDGEC and their matched controls.

Our results of reduced structural connectivity in HDGEC are consistent with previous studies reporting white-matter microstructure abnormalities in the connections between the putamen and sensorimotor areas in manifest HDGEC [Marrakchi-Kacem et al., 2013; Poudel et al., 2014] and in the CC [Di Paola et al., 2012, 2014; Phillips et al., 2013; Rosas et al., 2006, 2010]. However, in comparison with previous studies, in which white-matter tracts were segmented based on anatomical ROIs, we used brain activity maps from a motor fMRI task to localize the ROIs. This approach allowed us to restrict the analysis of white matter connections to functional meaningful regions, making possible to directly compare structural and functional connectivity measures to explore the relationship between them.

We found that only the motor CC structural connectivity of HDGEC significantly correlated with the functional connectivity between the areas connected by it, namely, the left and right SM1. This correlation remained significant when looking at the HDGEC manifest group alone. In the case of the left putamen–left SM1 tract, the correlation was still no significant when analyzing the manifest HDGEC group alone. This result rules out the possibility that the lack of correlation between functional and structural connectivity in premanifest HDGEC could be hindering a possible correlation in the manifest group. In healthy controls, no correlation was found between functional and structural connectivity in either tract. More concretely, our results show that reduced structural connectivity was significantly associated with reduced strength of functional connectivity in the motor CC of HDGEC. In contrast, no significant relationship between functional and structural connectivity was shown in the left putamen–left SM1 tract. The lack of correlation in this intrahemispheric tract is in line with a recent study that found no significant correlation between functional and structural connectivity between the left thalamus and the left sensory cortex in HD [Müller et al., 2016]. It should be noted, however, that there are important differences between the present study and the study of Müller et al. For example, Müller et al. chose the thalamus as a seed region as opposed to the putamen and they employed resting-state fMRI, whereas we studied the task-related functional connectivity of the motor circuit while participants performed a motor task. Müller et al. interpreted the lack of correlation between functional and structural connectivity as the result of individual differences in the ability to compensate the structural damage by adapting brain activity. However, another possible interpretation would be that the alterations in functional and structural connectivity are not necessarily coupled during all stages of neurodegeneration, and they may progress at different rates.

Previous studies using graph theory analyses on other neurodegenerative diseases have investigated the relationship between whole-brain structural connectivity and resting-state functional connectivity. In amyotrophic lateral sclerosis (ALS), functional and structural connectivity degeneration have been found to be coupled [Schmidt et al., 2014]. On the other hand, a decline in the coupling between functional and structural connectivity has been found in Alzheimer's disease patients when comparing them with healthy controls and amnestic mild cognitive impairment patients [Sun et al., 2014]. Recently, these types of analyses have been performed in premanifest HDGEC, showing a relationship between white-matter organization and functional connectivity during the prodromal phase [McColgan et al., 2017].

It still remains unknown how functional and structural alterations interplay during neurodegeneration and whether this is common across the different neurodegenerative diseases. On one hand, the functional consequences of structural alterations may depend on the degree of centrality of a given region, that is, the number of connections

that it has with other brain regions. It has been shown that lesions in the highest interconnected regions of the brain, often referred to as hubs, are more likely to be symptomatic than lesioned non-hubs [Crossley et al., 2014]. On the other hand, functional alterations can occur in the absence of detectable structural correlates [Damoiseaux and Greicius, 2009; Honey et al., 2009], possibly due to indirect structural connections or to abnormal neurotransmission that does not entail grey-matter or white-matter alterations [Rowe, 2010]. Furthermore, compensatory mechanisms are triggered by the neurodegenerative process, which may result in cell survival at the cost of network failure [Palop et al., 2006]. Different adaptive and maladaptive neural responses have been proposed to occur as a consequence of a pathological perturbation, such as compensation, neural reserve, and degeneracy in the first group, and diaschisis, transneuronal degeneration, and dedifferentiation on the latter one [Fornito et al., 2015]. Some of these responses can occur simultaneously and their evolution across time may be complex. In this regard, longitudinal studies can shed light on how neurodegeneration alters structure and function along different stages. HD is a potentially good model to study neurodegeneration longitudinally. In contrast with other neurodegenerative diseases, HD is known to be caused by a single gene mutation and genetic tests are available, which makes it possible to track the neurodegenerative process as the earliest stages in premanifest individuals.

This study presents some limitations that must be acknowledged. First, given the modest sample size, generalization of the results should be carried out cautiously. Second, the impossibility of virtually segmenting the motor CC in all of the patients reduced the number of data-points for the structural connectivity metrics of this white matter tract. Third, although we used DW-MRI indices as a measure of structural connectivity strength, it is important to bear in mind that the interpretation of these measures is ambiguous, as multiple sources, such as axon diameter, myelination, packing density, membrane permeability, and fiber orientation may account for differences observed in DW-MRI signal [Jones et al., 2013]. It has nevertheless been argued that it is a plausible hypothesis that at least part of the variance in DW-MRI metrics can be attributed to underlying differences in structural connectivity strength and DW-MRI measures have been found to be correlated with resting state functional connectivity in healthy individuals [Khalsa et al., 2014]. Last, future studies should study HDGEC longitudinally to better understand the progression of both functional and structural alterations during the different stages of HD.

CONCLUSION

The results of this study show that the motor circuit of HD patients is altered in terms of both functional and structural connectivity and that changes in striato-cortical pathways can affect cortico-cortical connections within the same interconnected network. We observe a dysfunction in the inhibitory interhemispheric functional connectivity of sensorimotor areas. Furthermore, a reduction in structural and functional connectivity is associated with more severe motor disability. Last, our results indicate that reduced interhemispheric functional connectivity is associated with a reduced structural connectivity of the motor CC of HDGEC. In contrast, in the case of the tract connecting the left putamen with the left sensorimotor cortex, no relationship between the reduced functional and structural connectivity was found. A possible explanation for this lack of correlation is that functional and structural abnormalities progress independently during some stages of neurodegeneration.

ACKNOWLEDGMENT

The authors are grateful to the patients and their families for their participation in this study and to Stephan Klöppel for his helpful comments in the process of analyzing the data of this study. We thank Adrià Vilà-Balló for his help in the earliest stages of this project.

REFERENCES

Adachi Y, Osada T, Sporns O, Watanabe T, Matsui T, Miyamoto K, Miyashita Y (2012): Functional connectivity between anatomically unconnected areas is shaped by collective network-level effects in the macaque cortex. Cereb Cortex 22:1586–1592.

Alexander GE, DeLong MR, Strick PL (1986): Parallel organization of functionally segregated circuits linking basal ganglia and cortex. Annu Rev Neurosci 9:357–381.

Allison JD, Meador KJ, Loring DW, Figueroa RE, Wright JC (2000): Functional MRI cerebral activation and deactivation during finger movement. Neurology 54:135–142.

Andersson JLR, Jenkinson M, Smith S, Andersson J (2007): Non-linear registration aka spatial normalisation FMRIB Technial Report TR07JA2.

Aramaki Y, Honda M, Sadato N (2006): Suppression of the non-dominant motor cortex during bimanual symmetric finger movement: A functional magnetic resonance imaging study. Neuroscience 141:2147–2153.

Ashburner J, Friston KJ (2005): Unified segmentation. NeuroImage 26:839–851.

Aylward EH, Sparks BF, Field KM, Yallapragada V, Shpritz BD, Rosenblatt A, Brandt J, Gourley LM, Liang K, Zhou H, Margolis RL, Ross CA (2004): Onset and rate of striatal atrophy in preclinical Huntington disease. Neurology 63:66–72.

Bartenstein P, Weindl A, Spiegel S, Boecker H, Wenzel R, Minoshima S, Conrad B (1997): Central motor processing in Huntington's disease: A PET study. 1553–1567.

Basser PJ, Pajevic S, Pierpaoli C, Duda J, Aldroubi A (2000): In vivo fiber tractography using DT-MRI data. Magn Reson Med 44:625–632.

Beaulé V, Tremblay S, Théoret H (2012): Interhemispheric control of unilateral movement. Neural Plast 2012:

Begeti F, Tan AYK, Cummins GA, Collins LM, Guzman NV, Mason SL, Barker RA (2013): The Addenbrooke?s Cognitive

Examination-Revised accurately detects cognitive decline in Huntington?s disease. J Neurol 260:2777–2785.
Beste C, Konrad C, Saft C, Ukas T, Andrich J, Pfleiderer B, Hausmann M, Falkenstein M (2009): Alterations in voluntary movement execution in Huntington's disease are related to the dominant motor system - Evidence from event-related potentials. Exp Neurol 216:148–157.
Bocci T, Hensghens MJM, Di Rollo A, Parenti L, Barloscio D, Rossi S, Sartucci F (2016): Impaired interhemispheric processing in early Huntington's Disease: A transcranial magnetic stimulation study. Clin Neurophysiol 127:1750–1752.
Bonelli RM, Hofmann P (2007): A systematic review of the treatment studies in Huntington's disease since 1990. Expert Opin Pharmacother 8:141–153.
Cohen J (1977): Statistical Power Analysis for the Behavioral Sciences. Academic Press.
Cole MW, Pathak S, Schneider W (2010): Identifying the brain's most globally connected regions. NeuroImage 49:3132–3148.
Crossley NA, Mechelli A, Scott J, Carletti F, Fox PT, Mcguire P, Bullmore ET (2014): The hubs of the human connectome are generally implicated in the anatomy of brain disorders. Brain 137:2382–2395.
Damoiseaux J, Greicius M (2009): Greater than the sum of its parts: A review of studies combining structural connectivity and resting-state functional connectivity. Brain Struct Funct 213:525–533.
Dell'Acqua F, Scifo P, Rizzo G, Catani M, Simmons A, Scotti G, Fazio F (2010): A modified damped Richardson–Lucy algorithm to reduce isotropic background effects in spherical deconvolution. NeuroImage 49:1446–1458.
Ferbert A, Priorit A, Rothwell JC, Day BL, Colebatchi JG, Marsden CD (1992): Interhemispheric inhibition of the human motor cortex. J Physiol 453:525–546.
Fischl B, Salat DH, Busa E, Albert M, Dieterich M, Haselgrove C, van der Kouwe A, Killiany R, Kennedy D, Klaveness S, Montillo A, Makris N, Rosen B, Dale AM (2002): Whole brain segmentation: Automated labeling of neuroanatomical structures in the human brain. Neuron 33:341–355.
Fling BW, Benson BL, Seidler RD (2013): Transcallosal sensorimotor fiber tract structure-function relationships. Hum Brain Mapp 34:384–395.
Fornito A, Zalesky A, Breakspear M (2015): The connectomics of brain disorders. Nat Rev Neurosci 16:159–172.
Friston K, Holmes AP, Poline JB, Grasby PJ, Williams SC, Frackowiak RS, Turner R (1995): Analysis of fMRI time-series revisited. NeuroImage 2:45–53.
Friston KJ, Buechel C, Fink GR, Morris J, Rolls E, Dolan RJ (1997): Psychophysiological and modulatory interactions in neuroimaging. NeuroImage 6:218–229.
Furtado S, Suchowersky O, Rewcastle NB, Graham L, Klimek M, Lou, Garber A (1996): Relationship between trinucliotide repeats and neuropathological changes in Huntington's diease. Ann Neurol 39:132–136.
Gavazzi C, Nave R, Della Petralli R, Rocca MA, Guerrini L, Tessa C, Diciotti S, Filippi M, Piacentini S, Mascalchi M (2007): Combining functional and structural brain magnetic resonance imaging in Huntington disease. J Comput Assist Tomogr 31: 574–580.
Grefkes C, Eickhoff SB, Nowak DA, Dafotakis M, Fink GR (2008): Dynamic intra- and interhemispheric interactions during unilateral and bilateral hand movements assessed with fMRI and DCM. NeuroImage 41:1382–1394.
Group HS (1996): Unified Huntington's disease rating scale: Reliability and consistency. Mov Disord 11:136–142.
Guo Z, Rudow G, Pletnikova O, Codispoti K-E, Orr BA, Crain BJ, Duan W, Margolis RL, Rosenblatt A, Ross CA, Troncoso JC (2012): Striatal neuronal loss correlates with clinical motor impairment in Huntington's disease. Mov Disord 27:1379–1386.
Harris GJ, Codori AM, Lewis RF, Schmidt E, Bedi A, Brandt J (1999): Reduced basal ganglia blood flow and volume in pre-symptomatic, gene-tested persons at-risk for Huntington's disease. Brain 122:1667–1678.
van den Heuvel MP, Sporns O (2011): Rich-club organization of the human connectome. J Neurosci 31:15775–15786.
Honey CJ, Honey CJ, Sporns O, Sporns O, Cammoun L, Cammoun L, Gigandet X, Gigandet X, Thiran JP, Thiran JP, Meuli R, Meuli R, Hagmann P, Hagmann P (2009): Predicting human resting-state functional connectivity from structural connectivity. Proc Natl Acad Sci USA 106:2035–2040.
Jenkins BG, Rosas HD, Chen Y-CI, Makabe T, Myers R, MacDonald M, Rosen BR, Beal MF, Koroshetz WJ (1998): 1H NMR spectroscopy studies of Huntington's disease: Correlations with CAG repeat numbers. Neurology 50:1357–1365.
Jenkinson M, Smith S (2001): A global optimisation method for robust affine registration of brain images. Med Image Anal 5: 143–156.
Jones DK, Knösche TR, Turner R (2013): White matter integrity, fiber count, and other fallacies: The do's and don'ts of diffusion MRI. NeuroImage 73:239–254.
Kassubek J, Juengling FD, Kioschies T, Henkel K, Karitzky J, Kramer B, Ecker D, Andrich J, Saft C, Kraus P, Aschoff AJ, Ludolph AC, Landwehrmeyer GB (2004): Topography of cerebral atrophy in early Huntington's disease: A voxel based morphometric MRI study. J Neurol Neurosurg Psychiatry 75: 213–220.
Khalsa S, Mayhew SD, Chechlacz M, Bagary M, Bagshaw AP (2014): The structural and functional connectivity of the posterior cingulate cortex: Comparison between deterministic and probabilistic tractography for the investigation of structure-function relationships. NeuroImage 102:118–127.
Klöppel S, Draganski B, Golding CV, Chu C, Nagy Z, Cook PA, Hicks SL, Kennard C, Alexander DC, Parker GJM, Tabrizi SJ, Frackowiak RSJ (2008): White matter connections reflect changes in voluntary-guided saccades in pre-symptomatic Huntington's disease. Brain 131:196–204.
Klöppel S, Draganski B, Siebner HR, Tabrizi SJ, Weiller C, Frackowiak RSJ (2009): Functional compensation of motor function in pre-symptomatic Huntington's disease. Brain 132: 1624–1632.
Langbehn DR, Brinkman RR, Falush D, Paulsen JS, Hayden MR (2004): A new model for prediction of the age of onset and penetrance for Huntington's disease based on CAG length. Clinical Genetics 65:267–277.
Leemans A, Jones DK (2009): The B-matrix must be rotated when correcting for subject motion in DTI data. Magn Reson Med 61:1336–1349.
Lehéricy S, Bardinet E, Tremblay L, Van de Moortele PF, Pochon JB, Dormont D, Kim D-S, Yelnik J, Ugurbil K (2006): Motor control in basal ganglia circuits using fMRI and brain atlas approaches. Cereb Cortex 16:149–161.
Leocani L, Cohen LG, Wassermann EM, Ikoma K, Hallett M (2000): Human corticospinal excitability evaluated with transcranial magnetic stimulation during different reaction time paradigms. Brain 1161–1173.

Liepert J, Dettmers C, Terborg C, Weiller C (2001): Inhibition of ipsilateral motor cortex during phasic generation of low force. Clin Neurophysiol 112:114–121.

MacDonald ME, Ambrose CM, Duyao MP, Myers RH, Lin C, Srinidhi L, Barnes G, Taylor SA, James M, Groot N, MacFarlane H, Jenkins B, Anderson MA WNS, Gusella JF, Bates GP, Baxendale S, Hummerich H, Kirby S, North M, Youngman S, Mott R, Zehetner G, Sedlacek Z, Poustka A, Frischauf AM, Lehrach H, Buckler AJ, Church D, Doucette-Stamm L, O'Donovan MC, Riba RL, Shah M, Stanton VP, Strobel SA, Draths KM, Wales JL, Dervan P, Housman DE, Altherr M, Shiang R, Thompson L, Fielder T, Wasmuth JJ, Tagle D, Valdes J, Elmer L, Allard M, Castilla L, Swaroop M, Blanchard K, Collins FS, Snell R, Holloway T, Gillespie K, Datson N, Shaw D, Harper PS (1993): A novel gene containing a trinucleotide repeat that is expanded and unstable on Huntington's disease chromosomes. Cell 72:971–983.

Marrakchi-Kacem L, Delmaire C, Guevara P, Poupon F, Lecomte S, Tucholka A, Roca P, Yelnik J, Durr A, Mangin JF, Lehéricy S, Poupon C (2013): Mapping cortico-striatal connectivity onto the cortical surface: A new tractography-based approach to study Huntington disease. PLoS One 8.

Matsui JT, Vaidya JG, Wassermann D, Kim RE, Magnotta VA, Johnson HJ, Paulsen JS, I, De Soriano Shadrick C, Miller A, E, Chiu Preston J, Goh A, Antonopoulos S, Loi S, Chua P, Komiti A, L, Raymond Decolongon J, Fan M, Coleman A, Christopher AR, Varvaris M, Ong M, Yoritomo N, Mallonee WM, Suter G, Samii A, Freney EP, Macaraeg A, Jones R, Wood-Siverio C, Factor SA, Barker RA, Mason S, Guzman NV, McCusker E, Griffith J, Loy C, McMillan J, Gunn D, Orth M, S, ??bmuth S, Barth K, Trautmann S, Schwenk D, Eschenbach C, Quaid K, Wesson M, Wojcieszek J, Guttman M, Sheinberg A, Law A, Karmalkar I, Perlman S, Clemente B, Geschwind MD, Sha S, Winer J, Satris G, Warner T, Burrows M, Rosser A, Price K, Hunt S, Marshall F, Chesire A, Wodarski M, Hickey C, Panegyres P, Lee J, Tedesco M, Maxwell B, Perlmutter J, Barton S, Smith S, Miedzybrodzka Z, Rae D, Vaughan V, D'Alessandro M, Craufurd D, Bek J, Howard E, Mazzoni P, Marder K, Wasserman P, Kumar R, Erickson D, Reeves C, Nickels B, Wheelock V, Kjer L, Martin A, Farias S, Martin W, Suchowersky O, King P, Wieler M, Sran S, Ahmed A, Rao S, Reece C, Bura A, Mourany L (2015): Prefrontal cortex white matter tracts in prodromal Huntington disease. Hum Brain Mapp 36:3717–3732.

McColgan P, Gregory S, Razi A, Seunarine KK, Gargouri F, Durr A, Roos RAC, Leavitt BR, Scahill RI, Clark CA, Tabrizi SJ, Rees G, the Track On -HD, Investigators the TO, Coleman A, Decolongon J, Fan M, Petkau T, Jauffret C, Justo D, Lehericy S, Nigaud K, Valabrègue R, Choonderbeek A, Hart EPT, Hensman MDJ, Crawford H, Johnson E, Papoutsi M, Berna C, Reilmann R, Weber N, Stout J, Labuschagne I, Landwehrmeyer B, Orth M, Johnson H (2017): White matter predicts functional connectivity in premanifest Huntington's disease. Ann Clin Transl Neurol 4:106–118.

Minkova L, Scheller E, Peter J, Abdulkadir A, Kaller CP, Roos RA, Durr A, Leavitt BR, Tabrizi SJ, Kloppel S (2015): Detection of motor changes in Huntington's disease using dynamic causal modeling. Front Hum Neurosci 9:634.

Müller H-P, Gorges M, Grön G, Kassubek J, Landwehrmeyer GB, Süßmuth SD, Wolf RC, Orth M (2016): Motor network structure and function are associated with motor performance in Huntington's disease. J Neurol 539–549.

Oldfield RC (1971): The assessment and analysis of handedness: The Edinburgh inventory. Neuropsychologia 9:97–113.

Palop JJ, Chin J, Mucke L (2006): A network dysfunction perspective on neurodegenerative diseases. Nature 443:768–773.

Di Paola M, Luders E, Cherubini A, Sanchez-Castaneda C, Thompson PM, Toga AW, Caltagirone C, Orobello S, Elifani F, Squitieri F, Sabatini U (2012): Multimodal MRI analysis of the corpus callosum reveals white matter differences in presymptomatic and early Huntington's disease. Cereb Cortex 22:2858–2866.

Di Paola M, Phillips OR, Sanchez-Castaneda C, Di Pardo A, Maglione V, Caltagirone C, Sabatini U, Squitieri F (2014): MRI measures of corpus callosum iron and myelin in early Huntington's disease. Hum Brain Mapp 35:3143–3151.

Park HJ, Friston KJ (2013): Structural and functional brain networks: From connections to cognition. Science 342:1238411.

Paulsen JS, Zimbelman JL, Hinton SC, Langbehn DR, Leveroni CL, Benjamin ML, Reynolds NC, Rao SM (2004): fMRI biomarker of early neuronal dysfunction in presymptomatic Huntington's disease. 51358:1715–1721.

Paulsen JS, Langbehn DR, Stout JC, Aylward E, Ross C. a, Nance M, Guttman M, Johnson S, MacDonald M, Beglinger LJ, Duff K, Kayson E, Biglan K, Shoulson I, Oakes D, Hayden M (2008): Detection of Huntington's disease decades before diagnosis: The Predict-HD study. J Neurol Neurosurg Psychiatry 79:874–880.

Penney JB, Vonsattel J-P, Macdonald ME, Gusella JF, Myers RH (1997): CAG repeat number governs the development rate of pathology in Huntington's disease. Ann Neurol 41:689–692.

Phillips O, Squitieri F, Sanchez-Castaneda C, Elifani F, Griguoli A, Maglione V, Caltagirone C, Sabatini U, Di Paola M (2015): The corticospinal tract in Huntington's disease. Cereb Cortex 25: 2670–2682.

Phillips OR, Joshi SH, Squitieri F, Sanchez-Castaneda C, Narr K, Shattuck DW, Caltagirone C, Sabatini U, Di Paola M (2016): Major superficial white matter abnormalities in Huntington's disease. Front Neurosci 10:

Phillips O, Sanchez-Castaneda C, Elifani F, Maglione V, Di Pardo A, Caltagirone C, Squitieri F, Sabatini U, Di Paola M (2013): Tractography of the corpus callosum in Huntington's disease. PLoS One 8:

Poudel GR, Stout JC, Domínguez D JF, Churchyard A, Chua P, Egan GF, Georgiou-Karistianis N (2015): Longitudinal change in white matter microstructure in Huntington's disease: The IMAGE-HD study. Neurobiol Dis 74:406–412.

Poudel GR, Stout JC, Domínguez D JF, Salmon L, Churchyard A, Chua P, Georgiou-Karistianis N, Egan GF (2014): White matter connectivity reflects clinical and cognitive status in Huntington's disease. Neurobiol Dis 65:180–187.

Reading SAJ, Yassa MA, Bakker A, Dziorny AC, Gourley LM, Yallapragada V, Rosenblatt A, Margolis RL, Aylward EH, Brandt J, Mori S, Van Zijl P, Bassett SS, Ross CA (2005): Regional white matter change in pre-symptomatic Huntington's disease: A diffusion tensor imaging study. Psychiatry Res Neuroimag 140:55–62.

Rosas HD, Lee SY, Bender AC, Zaleta AK, Vangel M, Yu P, Fischl B, Pappu V, Onorato C, Cha JH, Salat DH, Hersch SM (2010): Altered white matter microstructure in the corpus callosum in Huntington's disease: Implications for cortical "disconnection." NeuroImage 49:2995–3004.

Rosas HD, Tuch DS, Hevelone ND, Zaleta AK, Vangel M, Hersch SM, Salat DH (2006): Diffusion tensor imaging in presymptomatic and early Huntington's disease: Selective white matter pathology and its relationship to clinical measures. Mov Disord 21: 1317–1325.

Rosas HD, Goodman J, Chen YI, Jenkins BG, Kennedy DN, Makris N, Patti M, Seidman LJ, Beal MF, Koroshetz WJ (2001): Striatal volume loss in HD as measured by MRI and the influence of CAG repeat. Neurology 57:1025–1028.

Ross C. a, Aylward EH, Wild EJ, Langbehn DR, Long JD, Warner JH, Scahill RI, Leavitt BR, Stout JC, Paulsen JS, Reilmann R, Unschuld PG, Wexler A, Margolis RL, Tabrizi SJ (2014): Huntington disease: Natural history, biomarkers and prospects for therapeutics. Nat Rev Neurol 10:204–216.

Rowe JB (2010): Connectivity analysis is essential to understand neurological disorders. Front Syst Neurosci 4:1–13.

Scheller E, Abdulkadir A, Peter J, Tabrizi SJ, Frackowiak RSJ, Klöppel S (2013): Interregional compensatory mechanisms of motor functioning in progressing preclinical neurodegeneration. NeuroImage 75:146–154.

Schmidt R, Verstraete E, de Reus MA, Veldink JH, van den Berg LH, van den Heuvel MP (2014): Correlation between structural and functional connectivity impairment in amyotrophic lateral sclerosis. Hum Brain Mapp 35:4386–4395.

Smith SM (2002): Fast robust automated brain extraction. Hum Brain Mapp 17:143–155.

Sun Y, Yin Q, Fang R, Yan X, Wang Y, Bezerianos A, Tang H, Miao F, Sun J (2014): Disrupted functional brain connectivity and its association to structural connectivity in amnestic mild cognitive impairment and Alzheimer's disease. PLoS One 9:

Tabrizi SJ, Langbehn DR, Leavitt BR, Roos RA, Durr A, Craufurd D, Kennard C, Hicks SL, Fox NC, Scahill RI, Borowsky B, Tobin AJ, Rosas HD, Johnson H, Reilmann R, Landwehrmeyer B, Stout JC (2009): Biological and clinical manifestations of Huntington's disease in the longitudinal TRACK-HD study: Cross-sectional analysis of baseline data. Lancet Neurol 8:791–801.

Thieben MJ, Duggins a. J, Good CD, Gomes L, Mahant N, Richards F, McCusker E, Frackowiak RSJ (2002): The distribution of structural neuropathology in pre-clinical Huntington's disease. Brain 125:1815–1828.

Tzourio-Mazoyer N, Landeau B, Papathanassiou D, Crivello F, Etard O, Delcroix N, Mazoyer B, Joliot M (2002): Automated anatomical labeling of activations in SPM using a macroscopic anatomical parcellation of the MNI MRI single-subject brain. NeuroImage 15:273–289.

Weeks RA, Piccini P, Boecker H, Harding AE, Brooks DJ (1997): Cortical control of movement in Huntington ' s disease A PET activation study. Phys Med Biol 1569–1578.

Witt ST, Stevens MC (2013): The role of top-down control in different phases of a sensorimotor timing task: A DCM study of adults and adolescents. Brain Imaging Behav 7:260–273.